Off-axis re-entrant cavity ring-down spectroscopy with a mid-infrared continuous-wave optical parametric oscillator

**J. Peltola · M. Vainio · V. Ulvila · M. Siltanen ·
M. Metsälä · L. Halonen**

Abstract We demonstrate an off-axis cavity ring-down spectroscopy system, which uses a mid-infrared continuous-wave optical parametric oscillator as a light source. Off-axis injection with re-entrant configuration of the ring-down cavity is used to achieve high spectral resolution while maintaining high measurement speed. This makes the setup suitable for sensitive molecular spectroscopy in the mid-infrared region, particularly for studies that require high temporal resolution. Formaldehyde (H_2CO) absorption spectrum at 3.4 μm is measured using the off-axis re-entrant cavity ring-down spectrometer.

1 Introduction

Detection and quantification of trace gases is important for many scientific and industrial purposes, such as atmospheric monitoring [1], industrial process monitoring [2, 3], or medical diagnostics [4–6]. The development of optical methods [7, 8] has been increasing during the past few decades, because these are fast and need no pretreatment of the sample. In particular, cavity enhanced absorption spectroscopy (CEAS) is a powerful technique to measure low, parts per

J. Peltola · M. Vainio · V. Ulvila · M. Siltanen · M. Metsälä ·
L. Halonen (✉)
Laboratory of Physical Chemistry, Department of Chemistry,
University of Helsinki, P.O. Box 55, A.I. Virtasen aukio 1,
00014 Helsinki, Finland
e-mail: lauri.halonen@helsinki.fi
Fax: +358-9-19150279

M. Vainio
Centre of Metrology and Accreditation, P.O. Box 9, 02151 Espoo,
Finland

million (ppm) to parts per trillion (ppt), concentration levels [6, 8, 9]. Continuous-wave (cw) cavity ring-down spectroscopy (CRDS) is one of the most widely used CEAS techniques [10]. In the cw-CRDS method, continuous wave laser beam is coupled into an external optical cavity formed by two highly reflecting mirrors. If the light injection is interrupted, the intensity of light inside the cavity decays exponentially with a time constant τ [11, 12], which is called the ring-down time of the cavity. Without any absorbers inside the cavity, the ring-down time depends only on the reflectivity of the mirrors and the length of the cavity. In the presence of an absorber, the ring-down time is shorter due to the molecular absorption losses inside the cavity.

The absorption spectrum of the sample can be formed by plotting the inverse of the ring-down times as a function of frequency. The CRDS technique is independent of laser power fluctuations, since the decay time does not depend on the initial intensity of the light circulating in the cavity. Therefore, CRDS is a calibration-free technique if the line strength of the measured molecular transition is known. The effective absorption length and thus the sensitivity of the technique depends on the ring-down time of the empty cavity (τ_0). The smallest detectable absorption (α_{min}) can be calculated from τ_0 and its standard deviation (σ_0) [9]

$$\alpha_{min} = \frac{1}{c}\left(\frac{1}{\tau_0 - \sigma_0} - \frac{1}{\tau_0}\right), \tag{1}$$

where c is the speed of light. Real-time absorption measurements of trace gas samples require a technique that is both sensitive and fast. The spectral resolution of the conventional on-axis CRDS with a passive ring-down cavity (i.e., a cavity whose length (L) is not modulated) is limited by the free spectral range ($FSR = c/2L$) of the cavity. Normally, in the on-axis CRDS, the injected laser beam is mode matched to the lowest transverse electro-magnetic mode (TEM_{00})

of the cavity. Scanning of the laser without modulation of the cavity length leads to a transmission pattern where the recorded ring-down times are separated in frequency by the FSR. High spectral resolution hence requires a long cavity, which inevitably leads to large sample volume and a bulky instrument, or modulation of the cavity length. Length-modulated cavities are widely used with single frequency lasers [10, 13]. The repetition rate of the ring-down signals is then limited by the time response of the actuator used for the cavity length modulation. Many other techniques have also been proposed to increase the resolution and measurement speed of the conventional on-axis CRDS technique, such as: laser-locked CRDS system [14], fast frequency scanning of the laser [15], rapidly swept cavity design [16], or a combination of the cavity modulation and fast laser scanning approaches [17].

This paper reports off-axis light injection with re-entrant configuration [18, 19] of the ring-down cavity has been used. The off-axis technique provides enhancement of the spectral resolution without cavity length modulation [10, 20, 21]. It provides a simpler measurement setup than, for example, a laser-locked CRDS system [14], while maintaining a high signal repetition rate. We present an off-axis CRDS spectrometer based on a continuous-wave optical parametric oscillator (cw-OPO), which operates in the mid-infrared region (2.75–3.45 μm). Compared to visible diode lasers used in previous off-axis re-entrant CRDS works [20, 21], a mid-infrared cw-OPO operates in a wavelength range that is generally more useful for molecular spectroscopy, is widely tunable, and possesses a high output power. We have studied how variations of experimental parameters affect the performance of the spectrometer and have compared the sensitivity to that achieved by a conventional on-axis CRDS technique. Measurement of a formaldehyde (H_2CO) spectrum using our off-axis CRDS spectrometer is presented as a proof of concept.

Off-axis injection produces a dense or almost continuous cavity transmission pattern, owing to excitation of high order transverse electromagnetic (TEM) modes of the cavity. The re-entrant configuration is a special case, where the excited TEM modes form equally frequency-spaced groups of degenerate modes within the original FSR of the cavity. Thus, the cavity transmission spectrum is an equidistant comb, but more dense than in the case of on-axis injection. The theory of re-entrant configuration is discussed in more detail in Sect. 2. Off-axis injection was already studied by Herriott et al. [18] in the 60 s in the context of increasing the optical path length of multipass cells. With CEAS, the off-axis alignment was first used to increase the spectral resolution of integrated cavity output spectroscopy (ICOS) [22]. Paul et al. [20] presented the first off-axis CRDS setup in 2001. In 2010, J. Courtois et al. [21] reported a fast off-axis CRDS spectrometer based on a fast frequency-swept diode

laser in combination with the re-entrant configuration cavity operating in the 766 nm region.

2 Re-entrant condition and fractionally degenerated cavity

In the case of a cavity with off-axis injection, the propagation of light inside it can be described using ray optics and the ray transfer matrix method [18, 19, 23]. Consider a cavity, which is formed by two mirrors that are placed at a distance L apart and possess the same radius of curvature (ROC). In an xyz-coordinate system, where the z-axis is selected as the cavity optical axis, the transfer matrix T of one round trip in the cavity starting from a mirror surface is [19]

$$T = \begin{bmatrix} 1 - \frac{2L}{ROC} & 2L(1 - \frac{L}{ROC}) \\ -\frac{4}{ROC}(1 - \frac{L}{ROC}) & -\frac{2L}{ROC} + (\frac{2L}{ROC} - 1)^2 \end{bmatrix}$$
$$= \begin{bmatrix} A & B \\ C & D \end{bmatrix}. \tag{2}$$

The position and direction of the ray after N round trips can now be expressed using the transfer matrix T, the initial position x_0, and the direction (the angle between the light ray and the optical axis z) ϕ_0 on the rear mirror surface as

$$\begin{pmatrix} \varphi_N \\ x_N \end{pmatrix} = T^N \begin{pmatrix} \varphi_0 \\ x_0 \end{pmatrix}. \tag{3}$$

In the re-entrant condition, the off-axis injected beam returns to its starting point after N round trips. This condition is satisfied if the transfer matrix T^N (the Nth power of T) is an identity matrix. Using Sylvester's theorem [24] with $AD + BC = 1$ and $\cos \phi = (A + D)/2$, where A, B, C, and D are the elements of the transfer matrix T and ϕ is a variable in the Sylvester's theorem, we obtain the following condition for the cavity length for which a ray repeats itself after N round trips:

$$L_{\text{re-entrant}} = ROC\left[1 - \cos\left(\frac{K\pi}{N}\right)\right] \tag{4}$$

where K is an integer. Any stable resonator ($0 < g^2 < 1$, where $g = 1 - L/ROC$ is the geometric cavity parameter) that fulfills this condition can form a stable off-axis resonator. The eigenfrequencies $\nu_{q,mn}$ of a spherical resonator formed by two mirrors are given by [25]

$$\nu_{q,nm}^{\text{spherical}} = \frac{c}{2L}\left[q + (m + n + 1)\frac{\theta}{2\pi}\right], \tag{5}$$

where m and n are transverse mode indices and $\theta = 2\arccos(g)$ is the Goup phase shift of the TEM$_{00}$ mode.

Because, in standard cw-CRDS, the injected beam is mode-matched to the lowest transverse electro-magnetic mode (TEM$_{00}$) of the cavity, high order TEM modes can be

neglected and the difference between two adjacent eigenfrequencies $v_{q+1} - v_q = c/2L$ is the free spectral range of the cavity. Let us now consider a non-mode-matched re-entrant cavity, where high order TEM modes are also excited. The Gouy phase shift of the TEM_{00} mode for one round trip is $\theta = 2\pi K/N$. The cavity is stable when $0 < K/N < 1$. Thus, the eigenfrequency formula becomes

$$v_{q,nm}^{\text{spherical}} = \frac{c}{2LN}\big[Nq + (m+n+1)K\big]. \tag{6}$$

In this re-entrant condition, the cavity length provides degeneracy of transverse modes so that adjacent mode families are separated by $cK/2LN$. This divides the FSR of the cavity to N groups of degenerated and equidistant modes. The optical power is divided equally between the generated modes, each group of modes having $1/N^2$ of the initial power [19]. This reduces the signal at the cavity output by N times compared to mode-matched on-axis injection. Hence, the signal to noise ratio is reduced in a shot-noise limited setup by $\sqrt{N}$, but it is ideally compensated by the averaging of N times more measurable data points in the same time period. The re-entrant off-axis configuration therefore resembles the normal on-axis mode-matched situation, except that the transmission peaks of the cavity are more densely spaced in frequency. Therefore, the attainable resolution in a CEAS experiment is higher [21].

3 Experimental setup

The off-axis CRDS setup used in this work is schematically shown in Fig. 1. A continuous-wave singly resonant optical
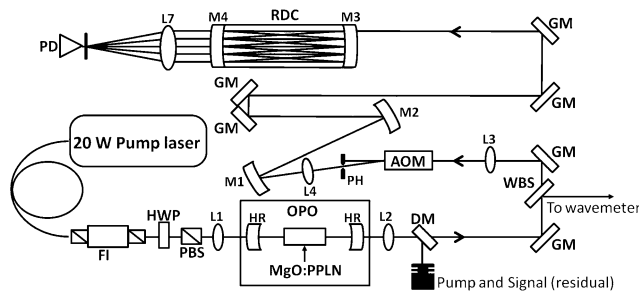

Fig. 1 Schematic of the experimental setup. The pump laser light is coupled into the OPO cavity through a Faraday isolator (FI) and a focusing lens L1. A combination of a half-wave plate (HWP) and a polarizing beam splitter (PBS) is used to control the pump power incident to the OPO. The OPO cavity consists of two highly reflective (HR) mirrors. MgO:PPLN is a MgO-doped, periodically poled lithium niobate crystal. Output beams are collimated using an uncoated CaF$_2$ lens L2. The mid-infrared idler beam is separated from the residual pump beam using dichroic mirror (DM). GM indicates a gold mirror. A small fraction of the idler beam is directed to a wavemeter using a wedge beam splitter (WBS). The idler beam is coupled into the acousto-optic modulator (AOM) through a focusing lens L3. PH is a pinhole. The idler beam is re-collimated after the AOM using lens L4 and directed through mode-matching mirrors (M1 and M2). The ring-down cavity (RDC) is formed by two highly reflective mirrors (M3 and M4). The light leaking out of the cavity is focused by lens (L7) on the photodetector (PD)

parametric oscillator is used as the light source. The cw-OPO can produce high output power in the wavelength region of 2.75–3.45 µm. A detailed description of the cw-OPO is presented in our previous papers [26, 27]. The OPO is pumped with a single-frequency Yb fiber laser system consisting of a seed laser (Koheras) and an optical amplifier (IPG YAR-20K-1064-LP-SF). The seed laser has a fast (up to 750 GHz s^{-1}) mode-hop-free tuning range of ∼100 GHz at 1064 nm. The maximum output power of the pump laser system is 20 W. The output beam of the pump laser is focused into a MgO-doped, periodically poled lithium niobate (MgO:PPLN) crystal using a plano-convex lens. The crystal is 1 mm thick and 50 mm long, and it has seven poling periods (from 28.5 to 31.5 µm). Both ends of the crystal are antireflection coated for the pump, signal, and idler wavelengths. The crystal is placed in a copper holder, the temperature of which can be stabilized to within ±6 mK anywhere between 20 °C and 120 °C using Peltier elements. Coarse tuning of the idler wavelength is done by choosing the poling period and temperature for the desired signal-idler pair. The fast mode-hop-free tuning of the seed laser is then converted to the idler region.

The OPO cavity is a simple two-mirror standing-wave resonator. Both mirrors are concave (ROC = 100 mm), highly reflecting at the signal wavelength (1550–1750 nm), and transmit at the pump and the idler wavelengths. Rear surfaces of the mirrors are antireflection coated for all three wavelengths. The idler beam exiting the resonator is collimated and separated from the residual pump and signal beams using a dichroic mirror. Typically, the single-mode output idler power used in this work is ∼100 mW.

A small fraction of the idler power is directed to a wavemeter (EXFO, WA-1500). The resolution of the wavemeter is ±60 MHz at the region of the idler frequency. The rest of the idler power is focused into an acousto-optic modulator (Isomet 1208-6M), which is used as an optical switch to interrupt light injection into the cavity so that a ring-down signal can be recorded. The first order diffraction maximum from the AOM is re-collimated and directed through mode-matching optics formed by two concave gold mirrors (M1 and M2). The purpose of the mode-matching optics is not to modify the beam properties to match the lowest transverse electro-magnetic mode of the ring-down cavity, but to re-shape the beam profile so that it excites as many high order TEM_{nm} $(n, m > 0)$ modes of the ring-down cavity as possible [28].

The ring-down cavity is formed by two concave mirrors (Layertec), which are placed on custom made mirror holders and connected to each other with a flexible stainless steel tube. The radius of curvature and the diameter of the mirrors are 1 m and 25.4 mm, respectively. Mirror reflectivity and the corresponding ring-down times over a 400 nm spectral range in the 3.3 micron region are shown in Fig. 2. The
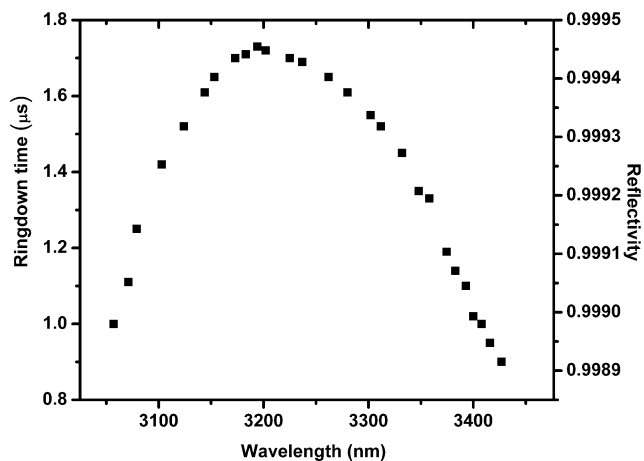
Fig. 2 Ring-down time of the 0.293 m long re-entrant CRDS cavity vs. wavelength, and the corresponding reflectivity of the cavity mirrors

Fig. 3 The transmission patterns of the re-entrant CRDS cavity when the OPO frequency is scanned over one FSR. **a** on-axis injection with FSR = 500 MHz. **b** Re-entrant off-axis injection with FSR $K/N = 125$ MHz with $K = 1$, $N = 4$

empty cavity decay time is approximately 1 μs at 2943 cm^{-1} with a 0.293 m long cavity, which corresponds to a finesse of about 3000. The rear surfaces of the mirrors are anti-reflection coated. The mirror holders are mounted to kinematic mirror mounts (Thorlabs, KC2/M), which are connected to each other by steel rods. Using this setup, we can adjust both the alignment of the mirrors and the length of the cavity. We have used $K = 1$ and $N = 4$ values, which gives the re-entrant length of 0.293 m. This results in an effective free spectral range (FSR$_{eff} = c/2LN$) of 125 MHz for the re-entrant cavity. For a normal non-degenerated cavity of this length, the FSR would be 500 MHz.

Formaldehyde tends to adsorb easily on surfaces. Because of that, the measurements were made in a continuous gas flow (∼1–2 liters per minute) [29]. The sample flow from the gas bottle (formaldehyde mixture of ∼10 ppm, AGA) to the cell is controlled using a mass flow controller (AREA, FC-785C). The ring-down cell is equipped with a Baratron pressure sensor (MKS, 622B). The measurements were recorded at the sample pressure of about 76 Torr (0.1 atm) and at room temperature. The pressure was chosen to demonstrate the performance of the off-axis CRDS system in conditions similar to those used in applications. In breath analysis, for example, sub-atmospheric pressures are often used to increase the selectivity of the measurement [4, 5]. The full width at half maximum (FWHM) of a pressure-broadened peak of formaldehyde at this pressure and at ∼3000 cm^{-1} is about 1 GHz. Using a normal passive on-axis CRDS system with an FSR of 500 MHz there would be only two measurable data points within this absorption profile.

The ring-down signal beam leaking out of the cavity is focused by a 15 cm lens on a photodetector (Vigo system, PVI-2TE-5/VPDC-20I). The signal from the detector is processed and digitized by a fast 14-bit data acquisition card (Gage, Compuscope 14100). The ring-down data are fitted
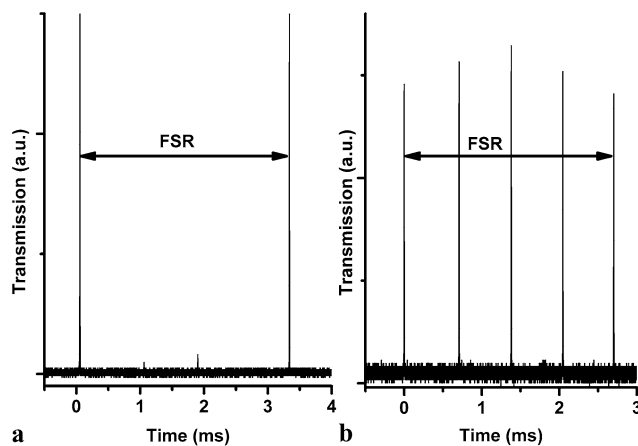
by the least-squares method to a single exponential function using the Levenberg–Marquadt algorithm [30] in a Lab-VIEW (National Instruments) program.

4 Results and discussion

In this section, we discuss the performance of our off-axis CRDS spectrometer. We demonstrate the use of the spectrometer for measuring narrow absorption lines of formaldehyde in the spectral region between 2943.08 and 2943.24 cm^{-1} (3397.62–3397.80 nm).

4.1 Performance of the spectrometer

Figure 3a shows the comb of transmission peaks of the CRDS cavity in the re-entrant configuration, but with conventional on-axis injection. Transverse modes other than TEM$_{00}$ are excited, but they contain only a small fraction of the total power due to the on-axis injection. In Fig. 3b, the injection is off-axis and the original FSR is divided into four groups of modes which are almost equally excited. The power of each generated mode depends on how much the off-axis the beam is injected into the cavity. The more the beam is aligned off the axis, the more evenly the power is distributed between the excited modes. A drawback of this, especially when the configuration is not re-entrant and the initial power is low, is such that the ring-down signal can become too weak to be detected and fitted reliably. This was not a problem because we used the re-entrant configuration and a high power light source. Another issue is that the beam pattern on the mirror surfaces depends on the off-axis alignment. Since the spatial size of the TEM modes on the mirror surface increases as the order of the TEM mode increases, the use of an alignment which is "too far" off-axis can cause

Fig. 4 Four scans over a group of degenerated transverse modes of the off-axis cavity ($K = 1$, $N = 4$, $R = 1.0$ m and $L = 0.293$ m) with four different cavity detunings. *Red circles* indicate split high TEM modes. The length deviation (ΔL) from the re-entrant length is **a** $\Delta L = 0$ μm, **b** $\Delta L = 254$ μm, **c** $\Delta L = 889$ μm, and **d** $\Delta L = 1.778$ mm
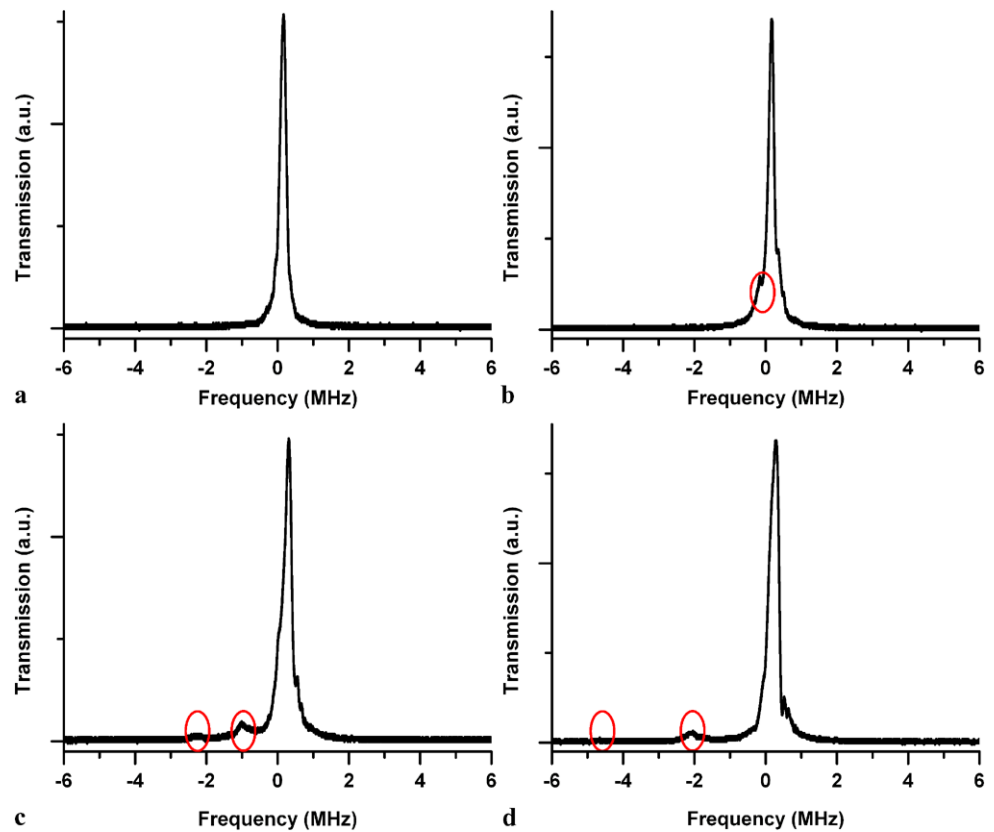

significant diffraction losses. The choice of the initial coordinates of the off-axis alignment is a compromise between adequately excited transverse modes and as low diffraction losses as possible. In practice, the off-axis alignment was done in the following steps: After finding a proper on-axis alignment, the beam was shifted in the horizontal (or vertical) direction (up to a few millimeters) off from the optical axis and tilted in the horizontal and vertical directions (typically a few milliradians) in a such a way that the groups of modes were approximately equally excited.

In addition to the proper amount of the off-axis alignment, the length of the CRDS cavity has to be carefully adjusted to achieve transverse mode degeneracy. We studied experimentally how sensitive the spectrometer is to the deviations of the cavity length (ΔL) from the optimum length ($L_{\text{re-entrant}}$) that corresponds to the re-entrant condition discussed in Sect. 2. The linewidth of a single transverse mode transmission peak of the cavity is approximately 200 kHz (FSR/finesse), and the short-term linewidth of the light source (OPO) is approximately 200 kHz. Therefore, the splitting of the degenerate transverse cavity modes should not exceed ~400 kHz in order to effectively fulfill the re-entrant configuration. As can be seen from the experimental data shown in Fig. 4, this corresponds to a maximum deviation of $\Delta L \sim 250$ μm for our cavity, which has $L_{\text{re-entrant}} = 293$ mm. The experimental uncertainty in the

cavity length adjustment is less than ± 100 μm, so the required accuracy in the cavity length is easy to achieve. It should be mentioned that in addition to ΔL, astigmatism of the cavity mirrors also leads to a splitting of mode degeneracy. The splitting breaks the actual degenerated mode into several degenerated sub-groups [21]. The sub-groups have a bell-shaped excitation envelope in frequency space and the envelope becomes wider as the injection is more off-axis. If the injection is relatively close to the optical axis and the astigmatism of the cavity mirrors is small, the effect can be on the order of a few hundred kHz [21]. The finesse of our cavity is not sufficient to make the mode splitting appear explicitly in the cavity transmission patterns.

Figure 5 shows a typical ring-down measurement of the re-entrant cavity. The red curve was recorded so that the OPO frequency was scanned over a cavity resonance without switching off the light injection. The observed ring-down signal shows oscillation, which is typical in cavity ring-down spectrometers based on narrow-linewidth (cw) light sources. The oscillation, or ringing, is caused by interference between the intracavity light field and the injected light field that has a varying frequency owing to frequency scanning. The amplitude of the ringing depends on the relative linewidths of the light source and the CRDS cavity, and it can be minimized by having a sufficiently fast frequency scan over the cavity resonance. In that case the
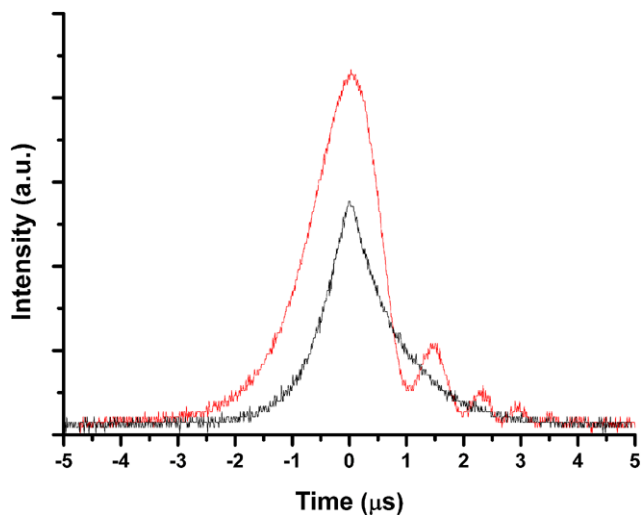
Fig. 5 Transient transmission patterns of the cavity in the time domain with a scanning speed of 740 GHz/s of the OPO frequency. *Red line* presents a scan without the AOM. *Black line* represents a scan with the AOM as an optical switch

Fourier transform limited linewidth of the light source becomes significantly larger than the cavity linewidth [21, 31]. In the case of a re-entrant off-axis cavity with partial splitting of the transverse mode degeneracy due to either cavity mirror astigmatism or deviation of the cavity length from the optimum, the ringing can also disappear owing to averaging of the transient excitation of incompletely degenerate transverse modes [21]. A potential advantage of such behavior is that light injection into the cavity does not have to be interrupted in order to attain a clean exponentially decaying ringdown signal, which is needed to accurately extract the time constant τ. With our experimental setup (OPO linewidth ∼200 kHz, ring-down time $\tau \sim 1$ μs), we did not observe an oscillation-free ring-down signal even at the fastest scanning speed of 740 GHz/s (Fig. 5). Hence, we used an AOM in all measurements reported here. The AOM switches off the light injection into the cavity after the optical power in the cavity reaches a certain trigger level. Regardless of the scanning rate, the ring-down signal observed with AOM switching is a clean exponential decay as exemplified by the black curve in Fig. 5.

The optimum trigger level for AOM switching depends on the splitting of transverse mode degeneracy caused by mirror astigmatism and other imperfections. This is illustrated in Fig. 6, which shows the relative ring-down time distributions of an empty cavity with two different AOM trigger levels. The data for the histograms were collected while modulating the OPO pump laser with a sinusoidal signal so that the OPO frequency was repeatedly scanned over the same transmission peak of the CRDS cavity. Red and black bars indicate positive and negative slopes of the sinusoidal scanning, respectively. The OPO pump laser frequency is increasing while the scanning slope is positive
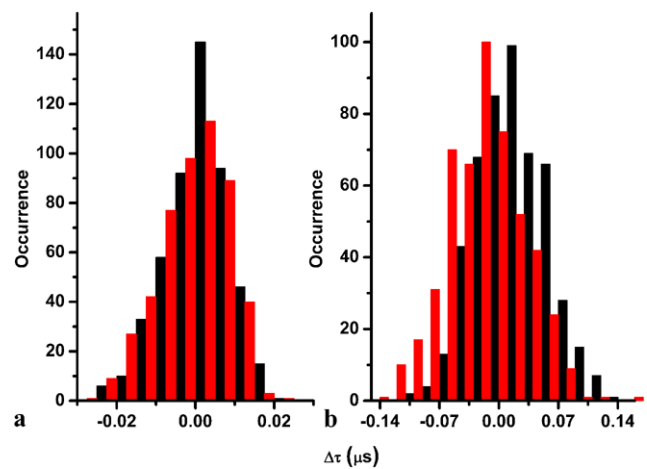
Fig. 6 Relative ring-down distributions of an empty cavity with different trigger levels of the AOM. $\Delta\tau = \tau - \bar{\tau}$, where $\bar{\tau}$ is the mean of the ring-down time distribution. *Red* and *black rectangles* indicate ring-down times for positive and negative slopes of the OPO frequency scan, respectively. The idler frequency was swept over one resonance peak of the cavity with a 40 Hz sinusoidal signal. Trigger level in picture (**a**) is close to the transmission maximum and in (**b**) close to the transmission minimum

and vice versa. In Fig. 6a, the trigger level was high and the AOM was triggered close to the transmission maximum of the cavity. In Fig. 6b, a low trigger level was used, i.e. the AOM was triggered almost right after the resonance occurred. As is seen from the figures, a small trigger level leads not only to a wider distribution of the ring-down times, but also to clearly different ring-down times depending on the direction of the frequency scan. This is attributed to imperfect transverse mode degeneracy. If the transverse modes of the cavity are not exactly degenerate, the timing of the excitation of the different modes is not uniform but depends on the direction of scanning. In the case of a positive slope (frequency is increasing), high order TEM modes are excited first. This is caused by the Gouy phase shift of the imperfectly degenerate re-entrant cavity, which shifts the high order TEM modes, such as $\upsilon_{q-1,13}$, to a lower frequency than the low order TEM modes like $\upsilon_{q,00}$. Because high order TEM modes in general have higher diffraction losses, the average of ring-down times is smaller for the scan with the positive slope (red bars, Fig. 6b). At very high scan speeds when the sweep over one transmission peak of the cavity is faster than the ring-down time, the effect of the trigger level becomes less important because the Fourier transform limited linewidth of the light source becomes dominant. In this case, more mode families contribute to the measurable ring-down signal, because they are excited almost simultaneously.

We used Allan deviation [32] to investigate of the optimum averaging time of the spectrometer. If the system is white (random) noise limited, the noise would decrease as $1/\sqrt{n}$ when the number of data points n increases. This is
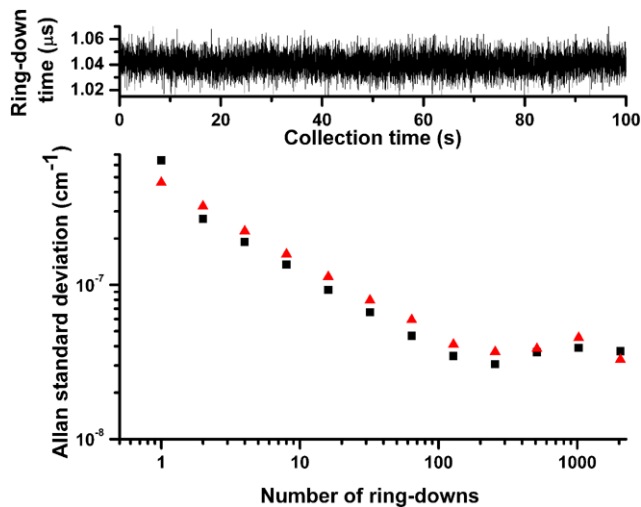
Fig. 7 The Allan deviation plots of the baseline of an off-axis CRDS (*red triangles*) and on-axis CRDS (*black squares*) instrument. The upper ring-down time data is from the off-axis measurement. The ring-down repetition rates were 120 Hz in both measurements. Both data were recorded at a total flow of air of 1–2 standard liters per minute and at the pressure of 0.1 atm
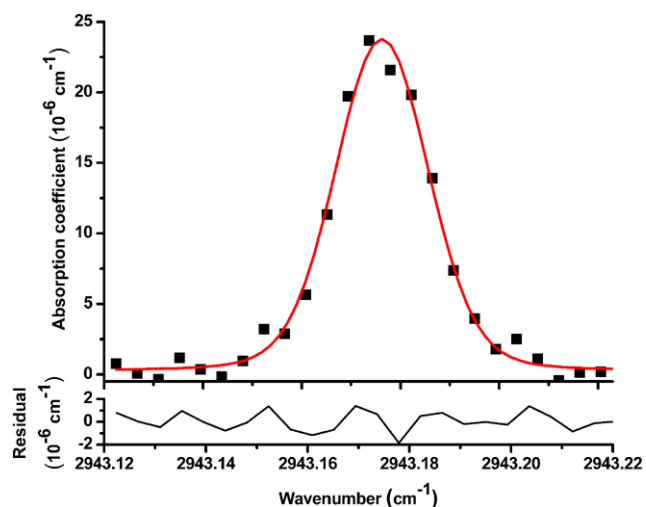

Fig. 8 A typical spectrum of H_2CO obtained by scanning the OPO frequency rapidly over the measured spectral region. *Solid markers* present measured data points (average of 50) and the *solid line* is a fit to them. The formaldehyde mixing ratio was approximately 10 ppmv. The pressure was 0.09 atm

illustrated as a linear negative slope in a $\log_{10}$–$\log_{10}$ plot of Allan deviation vs. n. Red triangle markers in Fig. 7 show a typical $\log_{10}$–$\log_{10}$ Allan deviation plot of $n = 12000$ ring-down segments of off-axis aligned re-entrant cavity with a constant flow of air. The OPO frequency is swept over one transmission peak of the re-entrant cavity by scanning the OPO pump laser with a 60 Hz sinusoidal wave. This corresponds to a repetition rate of 120 Hz for the ring-down events. As seen from the figure, the minimum detectable absorption (2σ) of $\sim4.0 \cdot 10^{-8}$ cm^{-1} is reached at the averaging time of ~2 s ($n = 240$). It should be mentioned that each degenerate group consist of different TEM modes and thus behaves slightly differently in the Allan deviation plot. The difference is small and is not crucial for the measurement of absorption spectrum of large spectral region as seen in Sect. 4.2. For comparison, we measured the Allan deviation for the mode-matched on-axis cavity. We used the same cavity with same conditions as in the off-axis measurement except that the beam was on-axis injected and mode-matched to the lowest TEM_{00} mode of the cavity. Black square markers in Fig. 7 show the respective Allan deviation. In this case, the achieved minimum detectable absorption (2σ) for 2 s averaging time was $\sim3.0 \cdot 10^{-8}$ cm^{-1}. With the current setup, there is no significant difference between the detection limit of the on-axis and the off-axis technique. The detection limit is also of the same order of magnitude as to what has been previously reported for an on-axis CRDS setup based on a mid-infrared cw-OPO [33] or other rather simple CEAS methods, such as optical-feedback cavity-enhanced absorption spectroscopy based on a mid-infrared quantum cascade laser at 4.43 µm [34]. Advantage of a cw-OPO is that it can
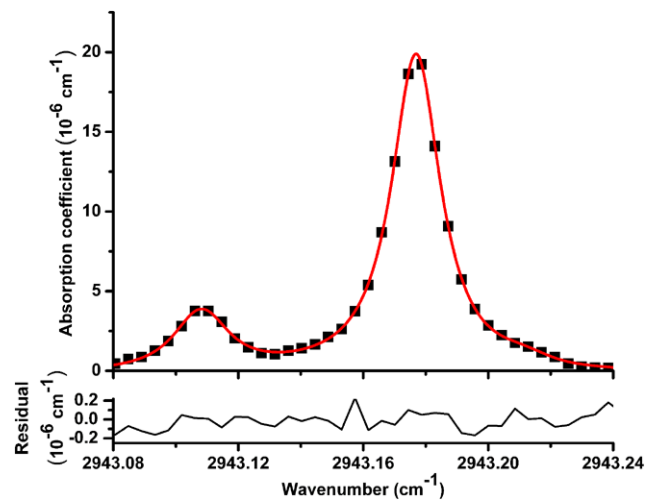
cover the spectral gap from 3 to 4 µm, where semiconductor lasers are not yet routinely available.

4.2 Spectroscopy of formaldehyde

We have used our spectrometer to measure the absorption spectrum of formaldehyde at 2943.08–2943.24 cm^{-1} (3397.62–3397.80 nm). The spectrum is shown in Fig. 8. The spectral region covers three rovibrational absorption lines of the ν_5 vibrational band (antisymmetric C–H stretch) [35]. According to the literature, the centers of the peaks are 2943.109, 2943.176, and 2943.215 cm^{-1} and the line strengths of these transitions are $0.567 \cdot 10^{-20}$, $1.736 \cdot 10^{-20}$, and $0.168 \cdot 10^{-20}$ cm/molecule, respectively [36]. The transition at 2943.176 cm^{-1} is a doublet. The idler frequency was repetitively scanned over the whole spectral region from 2943.08 to 2943.24 cm^{-1} by modulating the OPO pump laser frequency sinusoidally at the repetition rate of 2 Hz. The spectrum in Fig. 8 is an average of 50 scans (collection time 25 s). Three Voigt line shapes were fitted to the spectrum using the peak fitting software Fityk [37]. Below the spectrum is the fit residual, which is the difference between the measured points and the fitted Voigt line shapes. The standard deviation of the residual gives a minimum detectable absorption (2σ) of $1.9 \cdot 10^{-7}$ cm^{-1}.

Figure 9 shows an example of a spectrum of the strongest absorption peak of Fig. 8 measured with a single fast sweep (5 ms) of the idler frequency. The residual for the spectrum gives the minimum detectable absorption (2σ) of $\sim1.7 \cdot 10^{-6}$ cm^{-1} for a single sweep. This results in a detection limit of ~75 ppb for formaldehyde with a signal averaging time of 1 s. In comparison, J.H. Miller et al. [38] used

Fig. 9 A typical spectrum of H_2CO obtained from a single rapid (5 ms) scan over the measured spectral region. *Solid markers* present measured data points and *solid line* fitting. The formaldehyde mixing ratio was approximately 10 ppmv. The pressure was 0.1 atm

an off-axis integrated cavity output spectroscopy with an interband cascade laser for measuring a formaldehyde line at 2832.485 cm^{-1}. Their detection limit was 150 ppb with a data acquisition time of 3 s. It should be mentioned that the line strength of the transition at 2832.485 cm^{-1} is approximately two times stronger than that at 2943.176 cm^{-1}. A fast sweep of 5 ms over the specified wavenumber region corresponds to a repetition rate of 4.6 kHz for the ringdown events and thus, to a data-rate normalized minimum detectable absorption of $\sim 2.5 \cdot 10^{-8}$ cm^{-1} $Hz^{-1/2}$. To compare our fast single scan method with other work, we mention that Courtois et al. [21], using their fast-scanning off-axis CRDS setup, observed a minimum detectable absorption of 3×10^{-6} cm^{-1} and a data-rate normalized minimum detectable absorption of 1.6×10^{-8} cm^{-1} $Hz^{-1/2}$ for a data rate of 36 kHz. It should be mentioned that, although the sensitivity of our spectrometer is comparable to other simple off-axis CRDS setups, a lower data-rate normalized minimum detectable absorption can be achieved by using other simple cw-CRDS techniques. For example, the rapidly swept on-axis cw-CRDS approach in Ref. [39] yields $5 \cdot 10^{-10}$ cm^{-1} $Hz^{-1/2}$ at 4 kHz.

5 Conclusion

We have reported an off-axis cavity ring-down spectrometer using a mid-infrared continuous-wave optical parametric oscillator as a light source. The spectral resolution is enhanced by a factor of 4 when compared with a conventional passive on-axis CRDS system. The re-entrant configuration divides the original FSR of the cavity to 4 groups

of degenerated and equidistant modes. The instrument described in this paper is simple compared to, e.g., laser-locked CRDS instruments [14]. To our knowledge, this is the first time that a mid-infrared cw-OPO has been used as a light source for off-axis CRDS. A minimum detectable absorption of $\sim 1.7 \cdot 10^{-6}$ cm^{-1} was achieved with a single OPO sweep (5 ms) over an absorption peak of formaldehyde at 2943.176 cm^{-1}. This makes the setup suitable for fast real time measurements. A detection limit of 75 parts per billion (ppb) was achieved by measuring a formaldehyde absorption line at 2943.176 cm^{-1} with a data acquisition time of 1 s. For the future, the goal is to push the detection limit for formaldehyde down to 10 ppb, which would be desirable for breath and indoor air studies. For these applications, the sensitivity has to be improved by a factor of ten. This could be achieved by better cavity mirrors and by improving the mechanical stability of the re-entrant cavity. Also, a faster laser, e.g. a distributed Bragg reflector diode laser [40], for the OPO pump laser would increase the scanning speed of the OPO and thus enhance the performance of the spectrometer.

References

1. H. Fuchs, W.P. Dube, B.M. Lerner, N.L. Wagner, E.J. Williams, S.S. Brown, Environ. Sci. Technol. **43**, 7831 (2009)
2. G. Wysocki, A. Kosterev, F. Tittel, Appl. Phys. B, Lasers Opt. **80**, 617 (2005)
3. U. Willer, M. Saraji, A. Khorsandi, P. Geiser, W. Schade, Opt. Lasers Eng. **44**, 699 (2006)
4. C. Wang, P. Sahay, Sensors **9**, 8230 (2009)
5. F.M. Schmidt, M. Metsälä, O. Vaittinen, L. Halonen, J. Breath Res. **5**, 046004 (2011)
6. I. Ventrillard-Courtillot, T. Gonthiez, C. Clerici, D. Romanini, J. Biomed. Opt. **14**, 064026 (2009)
7. M.W. Sigrist, Rev. Sci. Instrum. **74**, 486 (2003)
8. B.A. Paldus, A.A. Kachanov, Can. J. Phys. **83**, 975 (2005)
9. G. Berden, R. Engeln, *Cavity Ring-Down Spectroscopy: Techniques and Applications* (Blackwell, Wiltshire, 2009)
10. D. Romanini, A.A. Kachanov, N. Sadeghi, F. Stoeckel, Chem. Phys. Lett. **264**, 316 (1997)
11. A. O'Keefe, D. Deacon, Rev. Sci. Instrum. **59**, 2544 (1988)
12. D.Z. Anderson, J.C. Frisch, C.S. Masser, Appl. Opt. **23**, 1238 (1984)
13. Y. He, B.J. Orr, Chem. Phys. Lett. **319**, 131 (2000)
14. R. Martínez, M. Metsälä, O. Vaittinen, T. Lantta, L. Halonen, J. Opt. Soc. Am. B **23**, 727 (2006)
15. Y. He, B.J. Orr, Appl. Phys. B, Lasers Opt. **79**, 941 (2004)
16. B.J. Orr, Y. He, Chem. Phys. Lett. **512**, 1 (2011)
17. I. Debecker, A. Mohamed, D. Romanini, Opt. Express **13**, 2906 (2005)
18. D. Herriott, H. Kogelnik, R. Kompfner, Appl. Opt. **3**, 523 (1964)
19. I.A. Ramsay, J.J. Degnan, Appl. Opt. **9**, 385 (1970)

20. J. Paul, L. Lapson, J. Anderson, Appl. Opt. **40**, 4904 (2001)
21. J. Courtois, A.K. Mohamed, D. Romanini, Opt. Express **18**, 4845 (2010)
22. G. Meijer, M.G.H. Boogaarts, R.T. Jongma, D.H. Parker, A.M. Wodtke, Chem. Phys. Lett. **217**, 112 (1994)
23. A. Gerrard, J.M. Burch, *Introduction to Matrix Methods in Optics* (Wiley, New York, 1975)
24. J.J. Sylvester, C. R. Acad. Sci. **XCIV**, 55 (1882)
25. O. Svelto, *Principles of Lasers* (Plenum Press, New York, 1998)
26. M. Vainio, J. Peltola, S. Persijn, F.J.M. Harren, L. Halonen, Opt. Express **16**, 11141 (2008)
27. M. Vainio, J. Peltola, S. Persijn, F.J.M. Harren, L. Halonen, Appl. Phys. B, Lasers Opt. **94**, 411 (2009)
28. D. Romanini, K.K. Lehmann, J. Chem. Phys. **105**, 10263 (1996)
29. Y. Mine, N. Melander, D. Richter, D.G. Lancaster, K.P. Petrov, R.F. Curl, F.K. Tittel, Appl. Phys. B, Lasers Opt. **65**, 771 (1997)
30. D.W. Marquardt, J. Soc. Ind. Appl. Math. **11**, 431 (1963)
31. F. Müller, G. von Basum, A. Popp, D. Halmer, P. Hering, M. Mürtz, F. Kühnemann, S. Schiller, Appl. Phys. B, Lasers Opt. **80**, 307 (2005)
32. D.W. Allan, Proc. IEEE **54**, 221 (1966)
33. S. Persijn, F.J.M. Harren, A. van der Veen, Appl. Phys. B, Lasers Opt. **100**, 383 (2010)
34. G. Maisons, P. Gorrotxategi Carbajo, M. Carras, D. Romanini, Opt. Lett. **35**, 3607 (2010)
35. L.R. Brown, R.H. Hunt, A.S. Pine, J. Mol. Spectrosc. **75**, 406 (1979)
36. The HITRAN 2008 database. http://www.hitran.com/
37. The FITYK software. www.unipress.waw.pl/fityk
38. J.H. Miller, Y.A. Bakhirkin, T. Ajtai, F.K. Tittel, C.J. Hill, R.Q. Yang, Appl. Phys. B, Lasers Opt. **85**, 391 (2006)
39. Y. He, B.J. Orr, Appl. Phys. B, Lasers Opt. **85**, 355 (2006)
40. D. Arslanov, S. Cristescu, F.J.M. Harren, Opt. Lett. **35**, 3300 (2010)